A study of the evaporation and condensation of *n*-alkane clusters and nanodroplets using quantum chemical methods

Vladimir M. Gun'ko,[a,b] Rasoul Nasiri,[a] Sergei S. Sazhin[*,a]

[a] *Sir Harry Ricardo Laboratories, School of Computing, Engineering and Mathematics, University of Brighton, Cockcroft Building, Lewes Road, Brighton BN2 4GJ, United Kingdom*
[b] *Chuiko Institute of Surface Chemistry, 17 General Naumov Street, Kiev 03164, Ukraine*

Abstract

The evaporation rate (γ) of *n*-alkane molecules in the C_8-C_{27} range from molecular clusters and nanodroplets is analysed using the quantum chemical solvation model (SMD) and the kinetic gas theory, assuming that the system is in a state of thermodynamic equilibrium (evaporation and condensation rates are equal). The droplet size, liquid density, evaporation enthalpy and Gibbs free energy of evaporation are calculated at 300-640 K. The quantum chemical calculations (SMD/HF or SMD/B3LYP methods with the 6-31G(d,p) basis set) are used to estimate changes in the Gibbs free energy during the transfer of a molecule from a liquid medium (clusters or nanodroplets) into the gas phase. The kinetic gas theory is used to estimate the collision rate of molecules/clusters/nanodroplets in the gas phase. This rate depends on partial pressures, temperature, sizes and masses of molecules and clusters/nanodroplets. An increase in the molecular size of evaporated alkanes from octane to heptacosane results in a strong decrease in the values of γ. Preliminary estimates of the evaporation/condensation coefficient, based on the direct analysis of the collisions of individual molecules with molecular clusters, are presented.

Keywords: Alkane droplet evaporation; Gibbs free energy; Evaporation rate; Evaporation coefficient; Quantum chemical modelling

Corresponding author. Phone +44 1273 642677 (Direct). Fax +44 1273 642330.
E-mail address: S.Sazhin@brighton.ac.uk

1 Introduction

Interest in the investigation of the evaporation of droplets has been stimulated by numerous industrial, technological, pharmaceutical and environmental applications [1-13]. Pioneering investigations of droplet evaporation were focused on water droplets due to their practical importance [4-8]. The droplet evaporation process affects the temperature behaviour of water or organic solvents and organic or inorganic solutes forming droplets of various sizes in the gas phase or on solid surfaces (e.g. inkjet or 3D polymer printing) [9-12]. The importance of this process in Diesel engines has been widely discussed in the literature [1-3,13]. The droplet evaporation processes have been studied using both experimental methods and theoretical modelling based on hydrodynamic and kinetic approaches [1-3,13-17].

The boundary condition for the kinetic region at the droplet surface was controlled by the evaporation coefficient. The values of this coefficient were calculated using the molecular dynamics (MD) approach in which the interaction between individual molecules was described by the force field (FF) methods, which simplify both inter- and inner-molecular interactions by ignoring electrons *per se* (quantum effects were ignored) [14,15,18-20]. Alternative quantum mechanical methods used to analyse the process of droplet evaporation were described in [21-23].

Most of the evaporation models were originally developed for water droplets. Despite the simplicity of water molecules in comparison with organics, the investigation of water evaporation is complex [4-8] due to strong hydrogen bonds between each atom in water molecules causing clustered water structures to be strongly affected by solutes and co-solvents [24,25]. These or similar effects are not observed in alkanes. The intermolecular bonds in alkanes are of the van-der-Waals (vdW) type [26]. This allows a certain simplicity of the modelling, including the application of molecular mechanics (MM) and molecular dynamics methods based on the vdW force field approach [16,18-20]. These models can be applied to both individual liquids and complex mixtures including a number of compounds which can be evaporated under various conditions [27-34]. However, the MD/FF models used to study evaporation of alkanes can

sometimes lead to erroneous results. The main sources of the errors in these models are related to the fact that changes in molecular polarisation, electron transfer and ion or radical formation, as well as electron factors at relatively high temperatures are ignored. Temperature increase can lead to strong thermal vibration of the bonds and changes in the electron density in atoms during vibrational excitations, fast rotations, conformational changes, and collisions between molecules. The electronic effects (enhanced at high temperatures) in intermolecular interactions between evaporated aromatics and organics with polar functionalities, in comparison with alkanes, can result in an increase in the errors in modelling of these systems using MD/FF, but investigation of aromatics is beyond the scope of this paper. In [23], a complex approach based on quantum chemical estimations of the Gibbs free energies of solvation (ΔG_s) and evaporation (ΔG_{ev}) and the kinetic gas theory was applied to analyse evaporation of real-life Diesel fuel clusters and nanodroplets, including a set of alkanes and substituted aromatics in the C_8-C_{27} range.

The processes considered in [23] are further investigated in the current paper. In contrast to [23], the present analysis is focused only on alkanes as the main components of Diesel fuel, and particularly on n-dodecane, the component widely used as a representative of this fuel. Also, a number of new processes, not investigated in [23], are discussed. These include molecule-molecule, molecule-cluster, and molecule-nanodroplet interactions, depending on temperature, kinetic energy, and orientation of the molecules hitting a droplet surface. The latter processes are expected to allow us to develop a better understanding of the underlying physics of the condensation/evaporation processes, described by the condensation/evaporation coefficient. As in [23] our analysis is based on the kinetic theory which allows us to apply our model mainly to molecular clusters and nanodroplets. Additional theoretical investigations, using *ab initio*, DFT and semiempirical quantum chemical methods, are performed to clarify the underlying physics of these processes.

2 Modelling methods

Individual molecules, clusters and nanodroplets of alkanes of the C_8-C_{27} range (including *n*-dodecane as a representative alkane) were studied using *ab initio* (HF/6-31G(d,p)), DFT (B3LYP/6-31G(d,p)) and semiempirical methods (PM6, PM7) implemented in the program packages: Gaussian 09 (revision D.01, 2013) [35], WinGAMESS (version May 1, 2013) [36,37], Firefly (version 8, June 2013) [38], and MOPAC 2012 (versions 13.238L and 13.238W, 2013) [39]. The geometry of initial nanodroplets (with 64 or 128 molecules) was optimised using the molecular mechanics program AMMP (modern full-featured molecular mechanics, dynamics and modelling program, with the CFF91 or MM+ force field method implemented in the VEGA ZZ program suit, version 3.0.1, 2013) [40]. After that, the geometry was optimised using the PM7 or PM6 methods. The HF and DFT methods with the 6-31G (d, p) basis set were applied to smaller systems with 7-8 molecules (molecular clusters). Visualisation of molecular structures was performed with the help of the ChemCraft 1.7/375 [41] or GaussView 5.09 [42] programs.

The Gibbs free energy of solvation (ΔG_s) was calculated using the solvation model (SMD, universal solvation model based on solute electron density and on a continuum model of the solvent defined by the bulk dielectric constant and surface tensions) developed by Truhlar *et al.* [43] and implemented in Gaussian 09 and WinGAMESS. N-dodecane was used as a solvent in SMD. The values of ΔG_s were used to estimate the changes in the Gibbs free energy upon evaporation (i.e. transfer of a molecule from the liquid phase into the gas phase where there is no solvation effect and $\Delta G_s = 0$).

The Gibbs free energy of solvation also was computed using OPLS-AA-L (Optimized Potentials for Liquid Simulations - All Atom for Long chain n-alkanes) force field [44] and dynamic simulation methods in which coupling and de-coupling of electrostatic and LJ interactions of an n-dodecane molecule with the rest of the system are taken into account [45]. 216 n-dodecane molecules were randomly placed into a cubic periodic box to model the liquid state. Two subsequent minimisations were made using the steepest descent of 1000 steps and

conjugate gradients of 9000 steps. Then after 1 ns molecular dynamics (MD) simulation, the system reached equilibrium state. The predicted value of density coincided with the one obtained from experimental data (745.0 kg/m^3 at 298.15 K) [46] (see also [44]). The length of the cubic simulation box was reduced from 6.2 nm to 4.3 nm during this simulation.

The MD simulations were carried out using the particle mesh Ewald method with grid spacing of 0.12 nm for the electrostatic interactions. A switch function was used for the analysis of the van der Waals interactions. Two values of cutoff, 1.1 nm and 1.3 nm, were used to smooth forces at the boundaries [47]. Dispersion effects, which can dominate at longer distances, were considered using corrections for energy and pressure [48]. The integration time step was selected as 2 fs, with the neighbours being updated every fifth step, using the cutoff distance of 1.5 nm. Periodic boundary conditions were used in all directions with a constant number of particles, constant pressure and constant temperature (NPT). The system was coupled to external constant temperature 298.15 K using the velocity rescaling algorithm with a time constant of 0.1 ps. Also, the pressure was coupled by Parrinello-Rahman barostat (1 atm, τ = 4 ps). Bonds and angles were flexible, except for the C-H bonds which were constrained using the LINCS algorithm [49].

When the equilibrium structure of n-dodecane molecules in the liquid phase was established, free energy perturbation (FEP) calculations were started to estimate the differences in the Gibbs free energy between different states of an n-dodecane molecule solvated in n-dodecane liquid using the Bennet Acceptance Ratio (BAR) technique [45]. In this method, the coupling factor λ, which changes from 0 to 1, shows fully de-coupled and coupled states for λ=0 and λ=1, respectively. This means that a molecule was transferred from an ideal gas environment to a fully solvated state when λ increased from 0 to 1 (eleven values of λ with equidistant spacing of 0.1 were chosen). Each state was simulated for 200 ps. Equilibrium was reached at 100 ps, which was followed by 100 ps (production phase) used for analysis. These FF simulations were carried out using the GROMACS-4.6.3 package [50].

To study the dynamics of elimination/condensation of molecules from clusters or nanodrops, the dynamic reaction coordinate (DRC) method was applied. In this method, one calculates atomic velocities (i.e. kinetic energy E_k) and potential energy E_p of the system and estimates the average temperature from the value of E_k. After each time step (chosen as $\Delta t = 10^{-16}$ s = 0.1 fs), the potential energy of the system is re-calculated using the PM7 method (MOPAC 2012) [39] or HF/6-31G(d,p) (WinGAMESS or Firefly) [36-38]. The trajectories of atoms are calculated using the classical mechanics approach adding the corresponding kinetic energies to atoms and re-calculating their velocity and coordinate vectors at each time step. These calculations allow one to model either the removal of a molecule from a cluster or nanodroplet, or its sticking to the cluster or nanodroplet, and to estimate the corresponding kinetic energies. This approach is useful for studying the interactions of molecules with nanodroplets depending on the orientation of the attacking molecules and the nanodroplet surface molecules, as well as the velocities of the attacking molecules.

The following equation for the evaporation rate ($\gamma_{i(i+j)}$) [21,22] was used in our analysis

$$\gamma_{i(i+j)} = b_{ij} \frac{p}{k_B T n_0} \exp\left(\frac{\Delta G_{i+j} - \Delta G_i - \Delta G_j}{k_B T} \right), \quad (1)$$

where n_0 is the initial number of molecules in a cluster or nanodroplet, $\gamma_{i(i+j)}$ is the evaporation rate of the ith-molecule from a cluster (or nanodroplet) $i+j$, b_{ij} is the collision rate of the ith molecule with the jth molecule (cluster/nanodroplet) [23], ΔG_{i+j}, ΔG_i, and ΔG_j are the Gibbs free energies of formation of the molecules (clusters/nanodroplets) from monomers (molecules) at the reference pressure p. If i or j refer to a monomer (in the gas phase) then the corresponding ΔG_i or ΔG_j are equal to zero. For other cases, $\Delta G_{i+j} - \Delta G_i - \Delta G_j$ corresponds to changes in the Gibbs free energy of the system due to attachment of the ith particle to the jth particle. Note that Expression (1) describes the actual rate of removal of molecules from the surface of the droplet, which is equal to the rate of condensing molecules in the equilibrium state. Expression (1) cannot be used directly for the analysis of evaporation of droplets in Diesel engine-like conditions, in

which the system is essentially not in the thermodynamically equilibrium state, but it can be applied to the analysis of some special experiments in which the state is close to thermodynamic equilibrium [51]. It can, however, be used for the analysis of some trends, which are observed in the immediate vicinity of Diesel fuel droplets where the state of the system is expected to be close to that of thermodynamic equilibrium [14-16].

As in [23], the collision rate between molecules/clusters/nanodroplets is estimated from the kinetic gas theory (KGT), assuming that these structures are in the state of thermodynamic equilibrium [17,21,22].

The evaporation enthalpy ($Q_{ev}(T) > 0$), contributing to ΔG_{ev}, and the density of liquids $\rho(T)$ as functions of temperature were estimated as described in [46]. $\rho(T)$ was used to estimate the size of clusters/nanodroplets at specific temperatures assuming that swelling of a cluster/nanodroplet is related to its decreased density.

We assume that the changes in the Gibbs free energy upon evaporation ($Q_{ev}(T) - T\Delta S = \Delta G_{ev} > 0$) correspond to the changes in the Gibbs free energy of a molecule upon solvation at temperature T_0 = 298 K but with the opposite sign as $\Delta G_{s,0} = \Delta H_s - T_0\Delta S < 0$, i.e. $\Delta G_{s,0} = -Q_{ev}(T_0) - T_0\Delta S$ at $\Delta H_s = -Q_{ev}(T_0)$. This leads us to the following equation

$$\Delta G_{ev}(T) = \Delta G_{s,0}(Q_{ev}(T) / \Delta G_{s,0} + T / T_0(1 + Q_{ev}(T_0) / \Delta G_{s,0})), \quad (2)$$

where $\Delta G_{s,0}$ is the Gibbs free energy of solvation determined using the SMD method under standard conditions. Eq. (2) was derived assuming that the changes in the entropy (ΔS) with temperature can be ignored.

In the case of thermodynamic equilibrium, the number of molecules held in the gas phase at temperature T can be described by the equation analogous to the Langmuir equation of adsorption [52]

$$\frac{n_{ev,i}}{n_0} = \frac{\alpha \frac{p_i}{p_0} \exp(-\Delta G_{ev,i}(T)/kT)}{1 + \frac{p_i}{p_0} \exp(-\Delta G_{ev,i}(T)/kT)}, \quad (3)$$

where α is a constant (determined from the limiting condition at a sufficiently high temperature), p_i/p_0 is the relative partial pressure of the ith evaporated component, p_0 is the total pressure, n_0 is the initial number of molecules in the droplet equal to the total number of molecules in liquid and gas phases during the evaporation process.

As mentioned earlier, the above analysis is applicable to the case when gas and liquid are in a state of thermodynamic equilibrium. When this is not the case, the relevance of quantum chemical effects is restricted mainly to the calculation of the evaporation coefficient

$$\beta = (f_{v,out} - f_{vr})/(f_{vs} - f_{vr}), \quad (4)$$

where f_{vs} is the distribution function of molecules leaving the liquid surface, assuming that the evaporation coefficient is equal to unity, f_{vr} is the distribution function of molecules reflected from the droplets. It was assumed that this coefficient is the same for all directions of the evaporated molecules [14,15]. The values of β for n-dodecane were estimated based on classical MD simulations [15]. As follows from these simulations, β decreases from 0.9-1.0 at T/T_c = 0.45-0.55 to 0.25 at T/T_c = 0.75-0.9, where T_c is the critical temperature. Direct reproduction of calculations presented in [24] but taking into account the quantum chemical effects does not look feasible at the moment.

In the next section, preliminary estimates of β will be performed based on the analysis of trajectories of individual molecules hitting the surfaces of molecular clusters, taking into account quantum chemical effects, or using MD/FF methods without consideration of these effects.

3. Results and discussion

The evaporation rate calculated using Eqs. (1) and (2), relative number of molecules evaporated from a droplet (n_{ev}/n_0) in equilibrium state, and residual number of molecules in a

nanodroplet during evaporation ($1 - n_{ev}/n_0$) versus nanodroplet diameters and temperatures, are shown in Figs. 1, 2 and 3, respectively. Parameter $n_{ev}(T)$ denotes the number of molecules transferred into the vapour phase as a function of temperature, n_0 is the total number of molecules, assuming that the system is in a state of thermodynamic equilibrium. Condition $n_{ev}/n_0 = 1$, or $1 - n_{ev}/n_0 = 0$, corresponds to complete evaporation of a nanodroplet occurring under equilibrium conditions at a certain temperature.

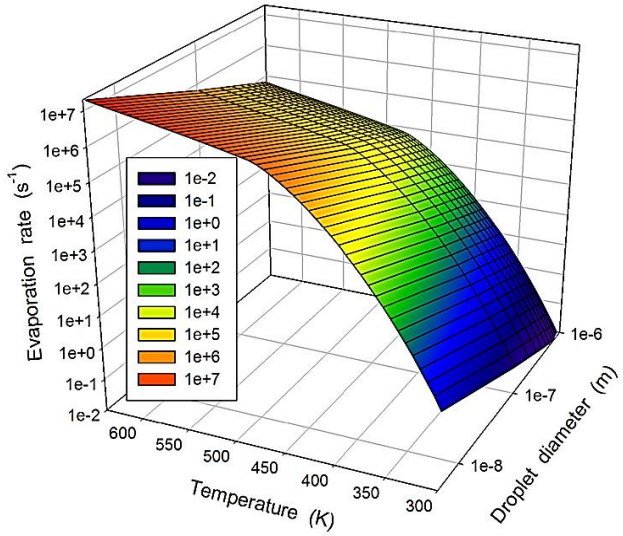

Fig. 1. Evaporation rate *vs*. temperature and nanodroplet diameter for evaporation of n-dodecane molecules from dodecane nanodroplets (HF/SMD/KGT with temperature dependent corrections and $\Delta G_s = -20.5$ kJ/mol at 300 K).

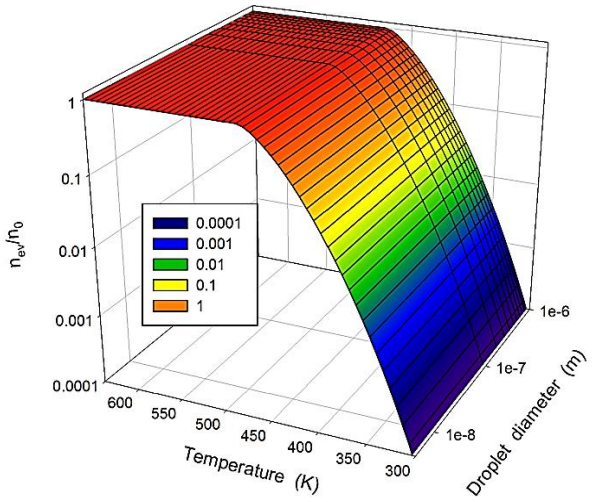

Fig. 2. Relative number of evaporated molecules *vs*. temperature and nanodroplet diameter for evaporation of n-dodecane molecules from n-dodecane nanodroplets (HF/SMD/KGT with temperature dependent corrections and $\Delta G_s = -20.5$ kJ/mol at 300 K).

The results shown in Figs. 1 and 2 refer to n-dodecane, while the results shown in Fig. 3 refer to a range of n-alkanes. Note that the results for droplets with diameters close to 1 μm, shown in Figs. 1 and 2, should be treated with caution, as for these relatively large droplets the condition of thermodynamic equilibrium is not likely to hold. An almost linear decrease in the values of γ with growing droplet diameters (Fig. 1) can be attributed to the fact that the ratio of volume to surface area of spherical nanodroplets is proportional to nanodroplet diameters.

Comparison of the Gibbs free energy of solvation of n-dodecane obtained by classical force field ($\Delta G_s = -30.9$ kJ/mol) and quantum chemical methods ($\Delta G_s = -20.5$ kJ/mol by

HF/SMD with WinGAMESS or −25.5 kJ/mol by DFT/SMD with Gaussian 09) shows that the FF result is closer to the experimental value, ΔG_s = –32.8 kJ/mol, than the SMD ones [43]. However, molecules are evaporated from a droplet surface but not from the bulk solution. At the surface, the number of n-dodecane molecule neighbours is about 5/8 of those in the bulk of the droplet for an ordered structure with non-bent molecules (simple estimation gives 32.8*5/8 = 20.5). Therefore, smaller values of $\Delta G_{i+j} - \Delta G_i - \Delta G_j = \Delta G_s$ (–20.5 or –25.5 kJ/mol) will be used in Eq. (1) for the calculations of the evaporation rate.

It follows, from Fig. 3, that large n-alkanes, such as icosane (C_{20}) and heptacosane (C_{27}), are more poorly evaporated than smaller n-alkanes (C_8, C_{12}) from n-dodecane medium. Evaporation of n-dodecane from n-octane medium (Fig. 3, C_{12}^{***}) occurs more slowly than from n-dodecane medium (C_{12}^{*}, C_{12}^{**}). In other words, we can expect that, as a result of evaporation, the gas phase consists mainly of n-octane from the C_{12}-in-C_8 system, while n-dodecane remains mainly in nanodroplets at $T < T_{b,C12}$ and evaporation of n-dodecane from octane droplets starts at $T \approx T_{b,C8} \approx 399$ K. This is expected to lead to an increase in mass fractions of compounds with larger molecular masses in complex hydrocarbon droplets during evaporation.

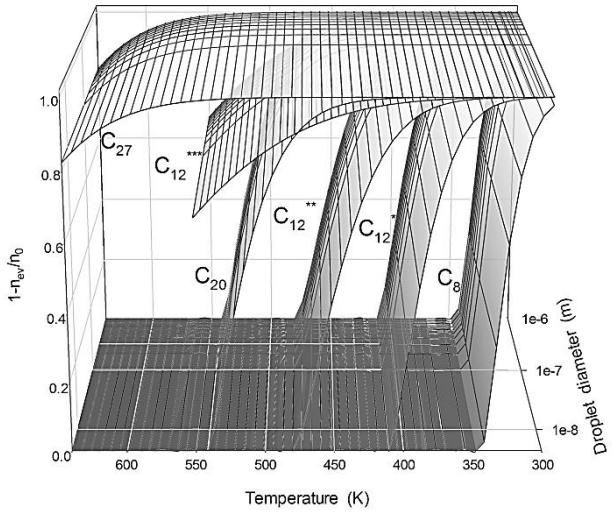

Fig. 3. Relative numbers of molecular residuals in a droplet as a function of temperature and droplet diameter for various n-alkanes evaporated from a nanodroplet with n-dodecane as a solvent calculated using the SMD/HF/6-31G(d,p)/KGT model (with $-\Delta G_s$ = 11.3 (C_8), 20.5 (C_{12}^{*}), 25.5 (C_{12}^{**}), 22.4 (C_{12}^{***} in the octane medium), 39.2 (C_{20}), and 55.1 (C_{27}) kJ/mol at 298 K).

Similar changes in droplet composition were observed for aromatics, in which the evaporation rate decreases with increasing molecular weight or the number of aromatic rings in the molecules [23]. According to Fig. 1, the composition changes can occur faster for smaller droplets. However, changes in n_{ev}/n_0 do not depend on the droplet sizes (see Figs. 2 and 3).

For small n-alkane molecules (C_6), evaporation of both monomers and dimers was observed, but for larger molecules (C_{16}), only monomers were evaporated [53]. This agrees with the modelling results for evaporation of monomers and dimers of various alkanes [23]. The difference in the evaporation of monomers and dimers can be related not only to the difference in their molecular weight but also to the difference in the corresponding values of Q_{ev}, ΔG_{ev} and ΔG_s.

The positive evaporation enthalpy Q_{ev} decreases with temperature; e.g. for n-dodecane, $Q_{ev} \approx 60$ kJ/mol and 18 kJ/mol at 300 K and 640 K, respectively. This leads to a decrease in the positive Gibbs free energy of evaporation ($\Delta G_{ev} > 0$) with temperature as intermolecular interactions in liquids decrease with temperature (liquid density and intermolecular bonds decrease when temperature increases). Therefore, the removal of a molecule from a heated droplet needs less energy than its removal from a cold droplet. The Gibbs free energy of solvation of molecules in liquid is negative ($\Delta G_s < 0$) and its modulus decreases with temperature due to the above-mentioned effect. The evaporation becomes more difficult when the size of evaporated molecules increases since this size affects the values of Q_{ev} [46], ΔG_{ev} and ΔG_s. For example, when the sizes of n-alkane molecules increase, their evaporation from nanodroplets with n-dodecane as a solvent, calculated using the SMD/KGT model, becomes more difficult (see Fig. 3) since the values of $|\Delta G_s|$ and ΔG_{ev} significantly increase with increasing molecular size of organics [23,46]. Evaporation of $C_8 - C_{12}$ n-alkanes from n-dodecane nanodroplets occurs mainly at $T < T_b = 489.5$ K (boiling temperature of dodecane) (see Fig. 3). An increase in the predicted values of $|\Delta G_s|$ for n-dodecane from 20.5 kJ/mol (SMD/HF) to 25.5 kJ/mol (SMD/DFT) leads to

a shift of the evaporation plot with temperature, as strong n-dodecane molecule-n-dodecane medium interaction (i.e. lower ΔG_s or higher $|\Delta G_s|$) slows down evaporation. The value of $|\Delta G_s|$ for heptacosane in n-dodecane is 55.1 kJ/mol (SMD/HF/6-31G(d,p)), much higher than that for C_8-C_{20}, and therefore the plot of $(1 - n_{ev}/n_0)$ for C_{27} shows the maximal shift towards higher temperatures (see Fig. 3).

The evaporation rates, expressed in terms of the rate of decrease of the squared droplet diameter if condensation is removed, (k_{ev}) versus temperature for droplets with diameters of 14.4 μm and 64 μm, are shown in Fig. 4. The plots shown in this figure are expected to show the trends of k_{ev} rather than their quantitative characteristics as the validity of the condition of thermodynamic equilibrium for such large droplets could be questionable. As follows from this figure, an increase in the droplet size leads to an increase in the evaporation rate; for droplets with d = 64 μm, k_{ev} increases with increasing temperatures. Similar effects were observed in the experiments, the results of which are described in [51]. In these experiments the evaporation rate of n-dodecane droplets was measured in a nitrogen atmosphere at 0.2 MPa at various temperatures.

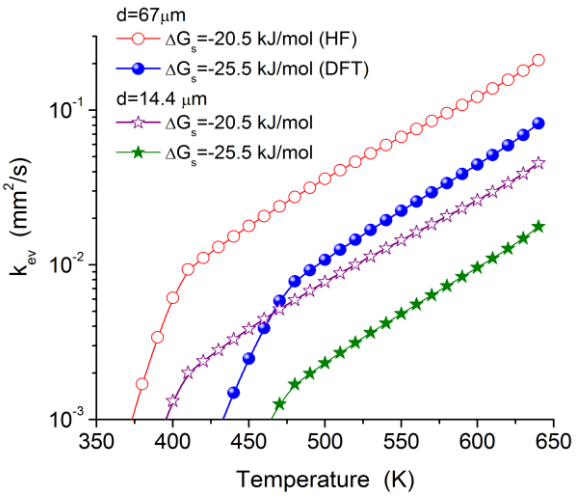

Fig. 4. The rates of evaporation of n-dodecane droplets with the initial diameters 14.4 and 67 μm and at two initial Gibbs free energies of solvation.

The average kinetic energy of the translational motion of the whole molecules (estimated as $E_k = 3k_BT/2$) in the temperature range 300-1200 K (E_k = 3.8-15.1 kJ/mol) is smaller than the

interaction energy of molecules in the liquid state at 300 K (ΔG_s = –25.5 kJ/mol, as predicted by SMD/B3LYP/6-31G (d,p)). Therefore, the evaporation of *n*-dodecane at 300-350 K is very slow (see Figs. 2 and 3). However, heating of nanodroplets at T > 400 K (see Figs. 1-4) leads to a decrease in the interaction (potential) energy between molecules and an increase in the average kinetic energy of the molecules (*vide infra*). Therefore, the probability that gas-phase molecules will stick to droplets is expected to decrease with increasing temperature due to two factors: increase in the average kinetic energy of molecules and decrease in the average interaction energy of the molecules (the modulus of the potential energy decreases). The molecule/nanodroplet scattering and evaporation of molecules from nanodroplets are determined by equilibrium conditions and the weight and diameters of nanodroplets, but do not depend on the kinetic characteristics of attacking molecules. However, the values and directions of velocities of attacking molecules relative to nanodroplet surfaces, as well as orientation of molecules at droplet surfaces, are expected to affect the collision processes, leading to scattering or condensation [54]. Also, evaporative cooling can reduce temperatures of nanodroplet surfaces which can result in an increase in condensation of molecules from the gas phase; this is consistent with experimental data [55].

In our analysis so far, the results of interaction of molecules with nanodroplets, determined by the evaporation/condensation rate (Eq. (1)), were obtained assuming the equilibrium state of the system in which the collisions between molecules and nanodroplets are described using the kinetic gas theory, regardless of the nature of these collisions. In what follows, the details of the collision processes are investigated using the dynamic reaction coordinate (DRC) method. The DRC results can elucidate the interaction mechanism of a molecule with a cluster/nanodroplet depending on the kinetic characteristics and temperature of the system. These characteristics refer to scattering or sticking of the molecules. In the DRC calculations, the total kinetic energy is partitioned into the kinetic energy of random thermal bond vibrations and rotations and the kinetic energy of the translational motion of the whole molecules.

In our analysis, the DRC method was applied to study the dependence of sticking/scattering of *n*-dodecane molecules on their angles of attack, kinetic energy (temperature), and cluster/nanodroplet size. The DRC calculations were performed for molecules interacting with a cluster (7 molecules) or a nanodroplet (64 or 128 molecules) of n-dodecane molecules. The results are shown in Figs. 5-7.

Figs. 5 and 6 show that at large angles of attack, a molecule is absorbed by a cluster or nanodroplet even of relatively small size (d = 2-7 nm) if the kinetic energy is low and the attacking molecule is not oriented exactly towards one of the surface molecules (but rather between neighbouring surface molecules) (see Fig. 5b). At $\Theta \approx 1^o$ (see Fig. 5a) an almost perfectly elastic collision was observed if the molecule had relatively high velocity (kinetic energy ~10 kJ/mol or larger) and was oriented directly towards one of the surface molecules.

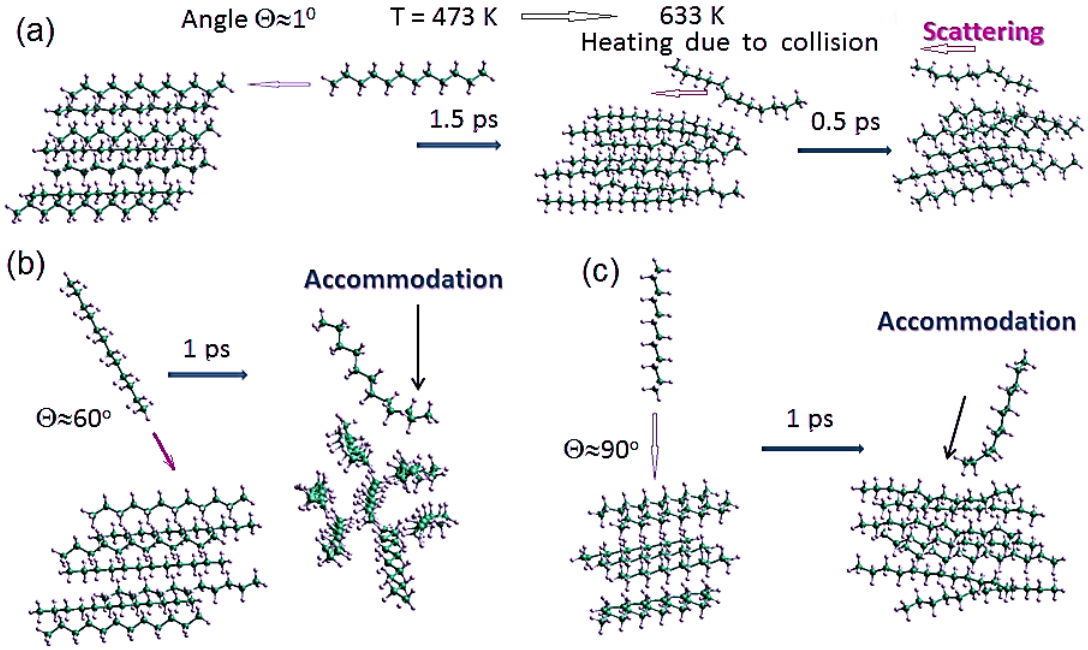

Fig. 5. Interaction of an n-dodecane molecule (hot, temperature ~1100 K) with a cluster of seven n-dodecane molecules (initial temperature 473 K; it increases due to the interaction with a hot molecule) at the angles of attack $\Theta \approx$ (a) 1^o, (b) 60^o and (c) 90^o.

In the DRC calculations shown in Figs. 5-7, the kinetic energy of the molecules in the clusters or nanodroplets was low and thermal vibrations and bond rotations corresponded to 300-400 K. At the same time, the kinetic energy of the attacking molecule was high (its effective temperature was in the range 500-1200 K).

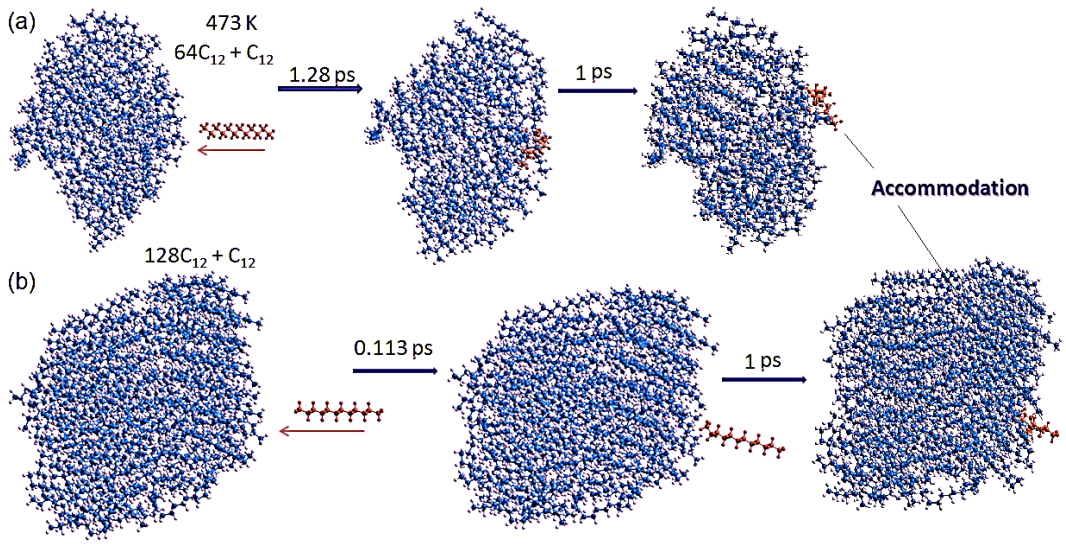

Fig. 6. Interaction of an *n*-dodecane molecule (hot, temperature ~1100 K) with clusters (initial temperature ~473 K) of (a) 64 and (b) 128 *n*-dodecane molecules at the angle of attack $\Theta \approx 90^{o}$.

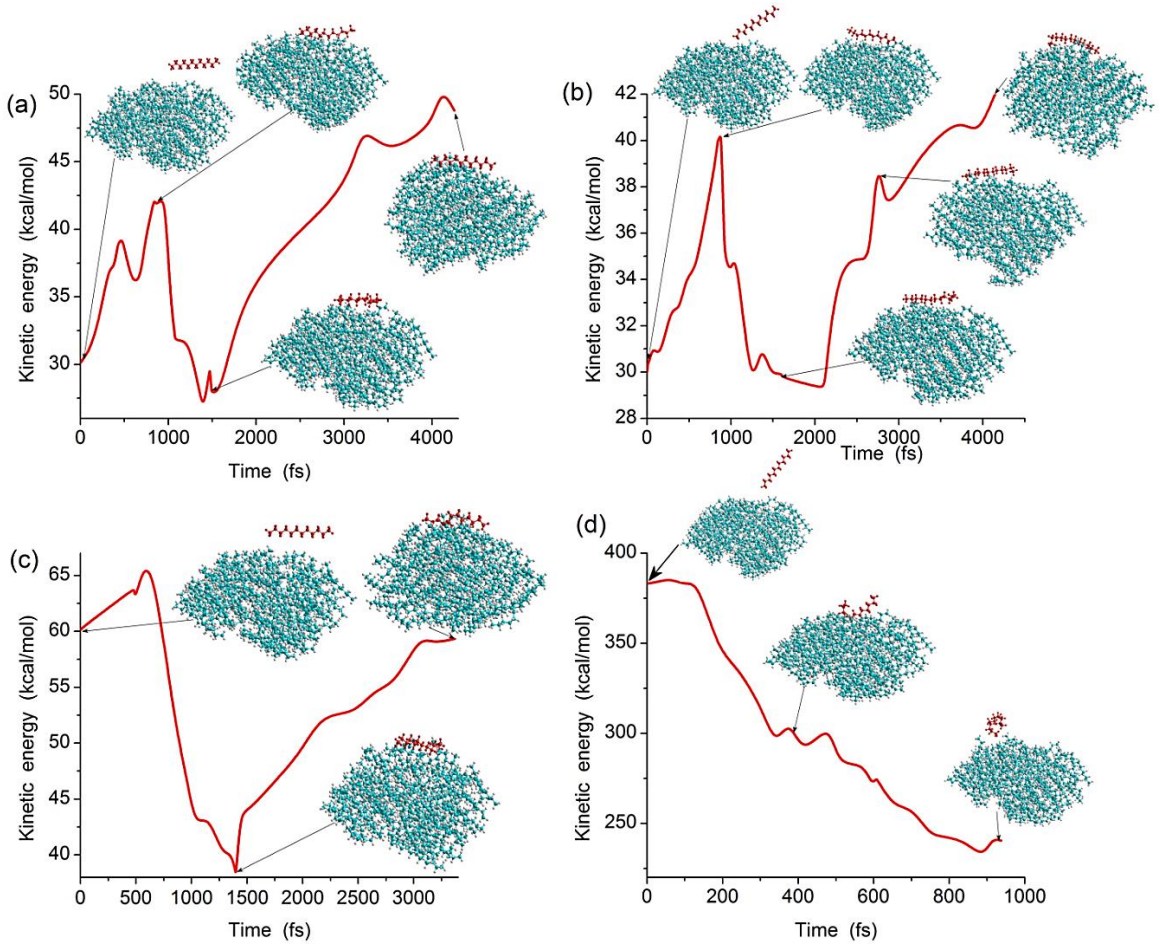

Fig. 7. Changes in the kinetic energy of the attacking n-dodecane molecule during its interaction with a nanodroplet of 64 n-dodecane molecules at various angles of attack: (a) 5^{o}, (b) 40^{o}, (c) 5^{o}, and (d) 45^{o}, and various initial kinetic energies: (a, b) 125.5, (c) 251, and (d) 1602 kJ/mol (these kinetic energies correspond to the energies of both translational motion and thermal vibrations or rotations).

At relatively low kinetic energies of attacking molecules (T < 450 K), the sticking (condensation) is expected to dominate over the scattering of molecules (see Fig. 7a-c), i.e., these molecules remain on the droplet surface following collisions after a certain time (3.7-4.5 ps in Fig. 7a-c). A significant increase in the kinetic energy of the attacking molecule after a minimum at 1.5-2 ps (Fig. 7a-c) is related to reorganisation of the nanodroplet after strong interaction with the attacking molecule accompanied by a decrease in its potential energy. An increase in the kinetic energy of the attacking molecules at the initial stage of the interactions (curves in Fig. 7a-c) is related to the reduction of the potential energy of the system when an attacking molecule approaches the cluster/nanodroplet. Then the kinetic energy of the attacking molecule decreases as it is transferred into the potential energy of the molecules in the cluster/nanodroplet. During the interaction of the high-energy scattered molecule with the cluster/nanodroplet (Fig. 7d), the kinetic energy of the system per molecule, E_k = 24.7 kJ/mol (including both translational motion and thermal vibrations/rotations), was close to $|\Delta G_{s,0}|$ = 25.5 kJ/mol at 298 K or Q_{ev} = 26.6 kJ/mol at 610 K. The kinetic energy of the system strongly decreases as the kinetic energy of the attacking molecule is transferred into the potential energy of the nanodroplet. Note that the interaction of a "hot" molecule ($T > T_b$) with a "cold" nanodroplet ($T < T_b$) leads to a decrease in the molecule's energy and a corresponding increase in the nanodroplet's energy, and then to the situation when the energies (temperatures) of both become close. The use of nanodroplets at high temperatures is restricted by their fast decomposition (see Fig. 8). The results of our calculations suggest that in the case where the attacking molecule is parallel or almost parallel to the droplet surface, the interaction between this molecule and the surface molecules takes place with many CH groups. Therefore, this interaction is expected to be maximal; i.e. the potential energy can be minimal at a certain distance between the molecule and the surface. Then, with the molecule approaching the surface, the potential energy grows strongly and the kinetic energy of the molecule decreases. This multi-centred interaction provides faster dissipation of the excessive

kinetic energy of a hot attacking molecule in the droplet in comparison with a uni-centred interaction (spear-type attack). Therefore, the probability of an attacking molecule sticking to the droplet is greater in the case of molecules approaching parallel or almost parallel to the droplet surface than for molecules attacking the droplet surface at high attacking angles.

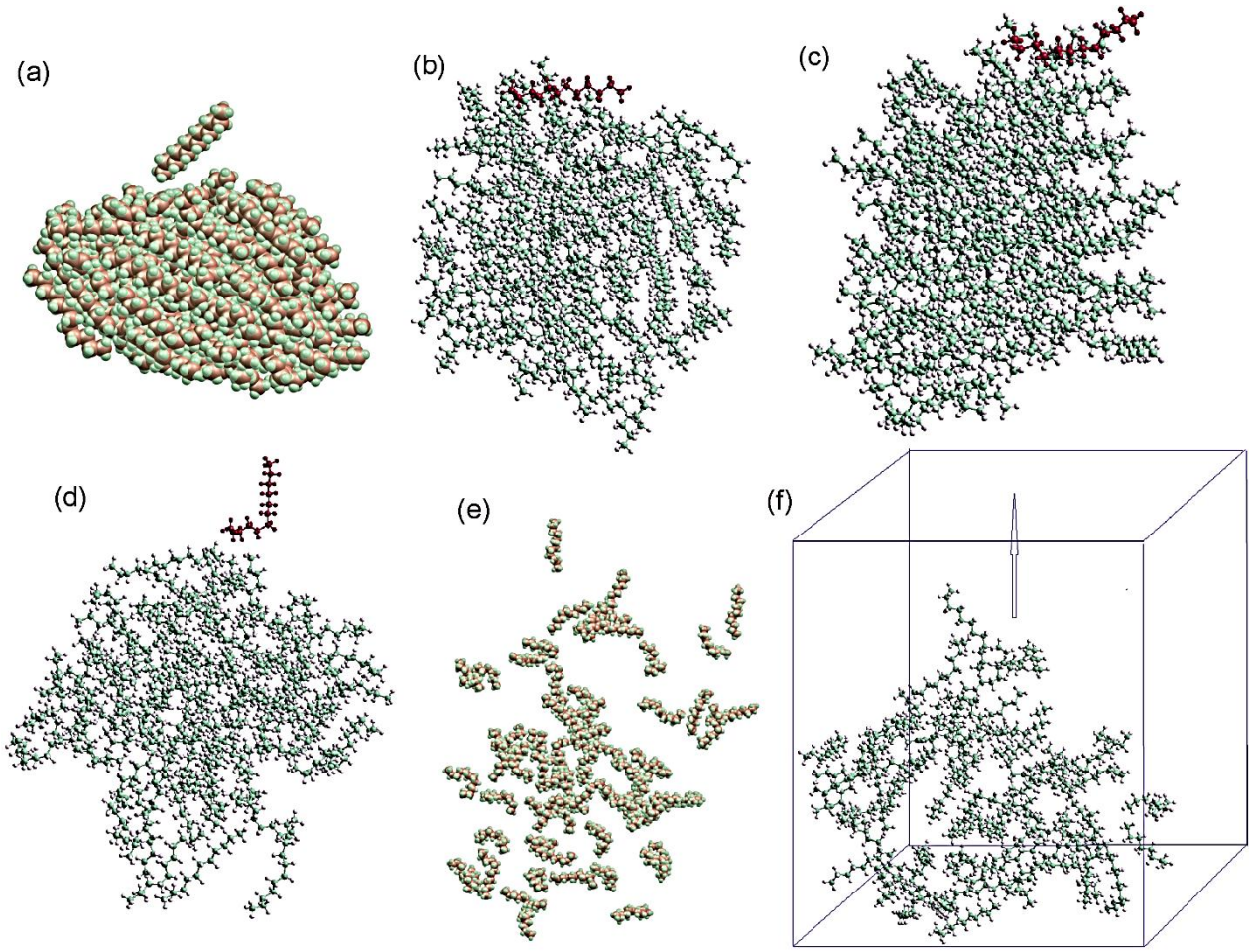

Fig. 8. Interaction of an n-dodecane molecule with a nanodroplet of 64 C_{12}: (a) initial geometry optimised with MM+; the system is heated (MD/FF(MM+)) for 5 ps at (b) 273 K, (c) 373 K, (d) 489.5 K (boiling temperature, T_b), (e) 773 K (with the value of E_k of the attacking molecule corresponding to the temperature of the system) in an infinite space and (f) in a box with periodic boundary conditions at the sides of the box, approximating a flat free surface at 473 K for the heating period 3.5 ps.

The process of the interaction between the attacking molecules and nanodroplets (with the initial geometry shown in Fig. 8a), heated at T = 273 K, 373 K, 489.5 K, and 773 K for 5 ps, is shown in Figs. 8b-e. In all cases, the initial kinetic energies of attacking molecules are equal to those of molecules in nanodroplets, and the nanodroplets are located in free unbounded space. As follows from Figs. 8b,c, the nanodroplet structures remain stable at 273 K and 373 K according to

MD/FF (MM+) calculations. In these cases, relatively cool attacking molecules are condensed at the nanodroplet surface, i.e. the condensation coefficient is close to unity. At n-dodecane boiling temperature (489.5 K), the nanodroplet starts to disintegrate into small clusters and individual molecules (see Fig. 8d). This decomposition of the nanodroplet into monomolecular and clustered fragments becomes more intensive at 773 K (see Fig. 8e).

To model the behaviour of larger structures and to analyse the evaporation process, a nanodroplet is located in a box with periodic boundary conditions at the sides of the box (Fig. 8f). The MD/FF calculations of such an n-dodecane system at 473 K show only slow removal of individual molecules. This result indicates that the condensation process can be less effective at T close to the boiling temperature than at lower temperatures. This corresponds to a decrease in the value of the condensation coefficient. Thus, the comparison of the mobility of molecules in nanodroplets in free space (Fig. 8a-e) and confined space (Fig. 8f) shows that the mobility of molecules is expected to reduce when the size of droplets increases. We can anticipate that the mechanisms of evaporation of large droplets (microdroplets) and nanodroplets are likely to involve rather different processes. In the case of microdroplets, individual C_{12} molecules are evaporated from their surfaces, while in the case on nanodroplets, they are disintegrated into clusters and individual molecules. This difference is attributed to different numbers of neighbouring molecules in clusters, nanodroplets and microdroplets, i.e. different numbers of intermolecular bonds per molecule, which should be broken to enable the removal (evaporation) of these structures from the nano- and microdroplets. As follows from our analysis, the accommodation time for the dynamic (DRC) interaction of a hot molecule (T > 500 K) with a nanodroplet is rather short. This time can be estimated using the Frenkel formula [52,56] for accommodation time (lifetime) of a molecule at a surface

$$\tau = \tau_0 \exp(E / k_B T), \qquad (5)$$

where $\tau_0 \approx$ 0.1-1.0 ps (time of molecular vibration), and E is the interaction energy. The value of E can be estimated as $E = Q_a - E_k$, where Q_a is the enthalpy of adsorption of a molecule at a

nanodroplet surface. If $Q_a = E_k$ in Eq. (5) then $\tau \approx \tau_0$, but structures shown in Fig. 7a-c are characterized by $\tau > \tau_0 \approx 0.1\text{-}1.0$ ps, i.e. $Q_a > E_k$. In the case shown in Fig. 7d, however, $\tau \approx 0.4$ ps and $Q_a < E_k$. If we assume that $Q_a \approx \Delta G_e$, then at 420 K, $\Delta G_e \approx 8.2$ kJ/mol, $E_k \approx 5.2$ kJ/mol, and $\tau \approx 0.24\text{-}2.4$ ps. If the accommodation time is longer than 0.24-2.4 ps at 420 K, then we can assume that a molecule is condensed at a nanodroplet.

As follows from the above-mentioned results, the condensation coefficient (i.e. the attachment of attacking molecules to a droplet surface) is expected to decrease with increasing temperatures of attacking molecules due to the increasing probability of scattering of attacking molecules at the clusters'/nanodroplets' surface. Also, the lifetime of the "surface" molecules exponentially decreases with temperature and the Gibbs free energy of evaporation decreases when the temperature of nanodroplets increases. These processes make additional contributions to the reduction of the condensation/evaporation coefficient with temperature. This decrease in the evaporation coefficient agrees with the prediction of the classical theory based on the MD simulations of *n*-dodecane molecules [15,16].

4. Conclusion

The evaporation/condensation processes in molecular clusters and nanodroplets of n-alkane molecules in the C_8-C_{27} range are investigated using quantum chemical methods (SMD/HF or SMD/B3LYP with the 6-31G(d,p) basis set). These methods were used to estimate changes in the Gibbs free energy during the transfer of a molecule from a liquid medium (clusters or nanodroplets) into the gas phase.

Evaporation rate (γ) is analysed using the above-mentioned quantum chemical solvation model (SMD) and the kinetic gas theory, assuming that the system is in a state of thermodynamic equilibrium (evaporation and condensation rates are equal). The evaporation rate is shown to decrease with increasing cluster/nanodroplet diameter and decreasing temperature. The relative number of evaporated molecules, however, does not depend on cluster/nanodroplet diameters,

and increases with increasing temperature. At certain temperatures, the clusters/nanodroplets are expected to fully evaporate. The relative number of residual molecules in clusters/nanodroplets for n-alkanes in the range C_8-C_{27} is shown to increase with temperature and the carbon numbers in the molecules. Thus the evaporation process of a mixture of n-alkanes is expected to lead to increased concentration of heavy n-alkanes in droplets.

The details of the collision processes of molecules with nanodroplets were investigated using the DRC method. The DRC calculations were performed for molecules interacting with a cluster (7 molecules) or a nanodroplet (64 or 128 molecules) of *n*-dodecane molecules.

It is shown that at large angles of attack (45-90^o), a molecule is absorbed by a cluster or nanodroplet even of relatively small diameter (d = 2-7 nm), if the kinetic energy is low (corresponding to $T < 473$ K) and the attacking molecule is not headed directly toward one of the surface molecules. The probability of the attacking molecule sticking to a droplet is maximal if the molecular plane is parallel or almost parallel to the droplet surface as this corresponds to multipoint interactions of relatively long dodecane molecule with the droplet surface. If the kinetic energy of the attacking molecules is high ($T > T_b$) then it is expected that it will scatter and be removed from the cluster/nanodroplet surface. Molecule-nanodroplet interaction results (sticking or scattering) depend on the kinetic energy (temperature) and orientations of the attacking molecule and surface molecules.

It is shown that the mechanisms of evaporation of microdroplets and nanodroplets are likely to involve rather different processes. In the case of microdroplets, individual C_{12} molecules are evaporated from their surfaces, while in the case of nanodroplets they can be disintegrated into clusters and individual molecules. The decrease in the evaporation/condensation coefficient with temperature, predicted by our analysis, agrees with the prediction of the classical theory based on the MD simulations of *n*-dodecane molecules.

Acknowledgment.

The authors are grateful to the EPSRC (UK) (grant EP/J006793/1) for their financial support.

Nomenclature and parameters

B3LYP	Exchange-correlation functional in DFT
DRC	Dynamic Reaction Coordinate
DFT	Density Functional Theory
FF	Force Field
HF	Hartree-Fock
KGT	Kinetic Gas Theory
MD	Molecular Dynamics
MM	Molecular Mechanics
PCM	Polarizable Continuum Model
PM6 and PM7	Semiempirical methods
SMD	Solvation model
ΔG_s	Gibbs free energy of solvation (kJ/mol)
ΔS	Entropy change (J/(K mol))
γ	Evaporation rate (s^{-1})
τ_0	Time of molecular vibration (s)
b_{ij}	Collision rate (s^{-1})
E_k	Kinetics Energy (kJ/mol)
E_p	Potential Energy (kJ/mol)
k_B	Boltzmann constant (1.3806488×10^{-23} J/K)
m_i	Molecular mass (atomic units, a.u.)
n_0	Initial number of molecule
n_{ev}	Number of evaporated molecules from a droplet
Q	Evaporation enthalpy (kJ/mol)
t	Time (s)
T	Temperature (K)

References

[1] J. Tamim, W.L.H. Hallett, Chemical Engineering Science 50 (1995) 2933–2942.

[2] A.M. Lippert, R.D. Reitz, SAE Technical Paper, (1997) 972882.

[3] W.L.H. Hallett, Combustion and Flame 121 (2000) 334–344.

[4] I. Langmuir, Journal of American Chemical Society 37 (1915) 417–458.

[5] I. Langmuir, Physical Review 12 (1918) 368-370.

[6] H.G. Houghton, Physics 4 (1933) 419-424.

[7] R.S. Bradley, M.G. Evans, R.W. Whytlaw-Gray, Proceedings of the Royal Society of London A 186 (1946) 368-390.

[8] G.D. Kinzer, R. Gunn, Journal of Meteorology 8 (1951) 71-83.

[9] R.D. Deegan, Phys. Rev. E 61 (2000) 475-485.

[10] B.J. de Gans, P.C. Duineveld, U.S. Schubert, Advanced Materials 16 (2004) 203-213.

[11] V. Dugas, J. Broutin, E. Souteyrand, Langmuir 21 (2005) 9130-9136.

[12] P.K. Wright, 21st Century Manufacturing, Prentice-Hall Inc., New Jersey, 2001.

[13] G.-S. Zhu, R.D. Reitz, International Journal of Heat and Mass Transfer 45 (2002) 495–507.

[14] B.-Y. Cao, J.-F. Xie, S.S. Sazhin, Journal of Chemical Physics 134 (2011) 164309(1-9).

[15] J.-F. Xie, S.S. Sazhin, B.-Y. Cao, Physics of Fluids 23 (2011) 112104(1-11).

[16] S.S. Sazhin, Progress in Energy and Combustion Science 32 (2006) 162-214.

[17] S. Chapman, T.G. Cowling, The Mathematical Theory of Nonuniform Gases, Cambridge University Press, Cambridge, 1970.

[18] H. Mizuguchi, G. Nagayama, T. Tsuruta, Seventh International Conference on Flow Dynamics, Sendai, Japan, 2010, p. 386.

[19] J.-F. Xie, S.S. Sazhin, I.N. Shishkova, B.-Y. Cao, Proceedings of International Symposium on Advances in Computational Heat Transfer (1-6 July, 2012 Bath, UK). CD, Begell House Inc., paper CHT12-MP02 (2012).

[20] J.-F. Xie, S.S. Sazhin, B.-Y. Cao, Journal of Thermal Science and Technology 7 (2012) 288-300.

[21] I. K. Ortega, O. Kupiainen, T. Kurtén, T. Olenius, O. Wilkman, M. J. McGrath, V. Loukonen, H. Vehkamäki, Atmospheric Chemistry and Physics 12 (2012) 225–235.

[22] O. Kupiainen, I.K. Ortega, T. Kurtén, H. Vehkamäki, Atmospheric Chemistry and Physics 12 (2012) 3591-3599.

[23] V.M. Gun'ko, R. Nasiri, S.S. Sazhin, F. Lemoine, F. Grisch, Fluid Phase Equilibria 356 (2013) 146–156.

[24] M. Chaplin, Water structure and science, http://www.lsbu.ac.uk/water/.

[25] V.M. Gun'ko, V.V. Turov, Nuclear Magnetic Resonance Studies of Interfacial Phenomena, CRC Press, Boca Raton, 2013.

[26] C.A. Hunter, Chemical Science 4 (2013) 834-848.

[27] P.v.R. Schleyer (Ed.), Encyclopedia of Computational Chemistry, John Wiley & Sons, New York, 1998.

[28] P.W. Atkins, R. Friedman, Molecular Quantum Mechanics, Fourth edition, Oxford University Press, Oxford, 2005.

[29] COSMOthermX, Version C30_1301, December 12th, COSMOlogic GmbH & Co. KG, Leverkusen, Germany, 2012.

[30] Y. Fujitani, K. Saitoh, A. Fushimi, K. Takahashi, S. Hasegawa, K. Tanabe, S. Kobayashi, A. Furuyama, S. Hirano, A. Takami, Atmospheric Environment 59 (2012) 389-397.

[31] S. Dirbude, V. Eswaran, A. Kushari, Atomization and Sprays 21 (2011) 787-798.

[32] G. Guéna, C. Poulard, A.M. Cazabat, Colloids and Surfaces A: Physicochemical and Engineering Aspects 298 (2007) 2-11.

[33] M. Heldmann, T. Knorsch, M. Wensing, SAE International Journal of Engines 6 (2013) 1213-1221.

[34] L. Zigan, I. Schmitz, A. Flügel, M. Wensing, A. Leipertz, Fuel 90 (2011) 348-363.

[35] M.J. Frisch, et al., Gaussian 09, Revision D.01, Gaussian, Inc., Wallingford CT, 2013.

[36] M.W. Schmidt, K.K. Baldridge, J.A. Boatz, S.T. Elbert, M.S. Gordon, J.J. Jensen, S. Koseki, N. Matsunaga, K.A. Nguyen, S. Su, et al. J. Comput. Chem. 14 (1993) 1347-1363.

[37] M.S. Gordon, M.W. Schmidt, In: C.E. Dykstra, G. Frenking, K.S. Kim, G.E. Scuseria (Eds.), Theory and Applications of Computational Chemistry, the First Forty Years, Elsevier, Amsterdam, 2005, pp. 1167-1189.

[38] A.A. Granovsky, Firefly version 8, www http://classic.chem.msu.su/gran/gamess/index.html.

[39] J.J.P. Stewart, MOPAC 2012, Versions 13.123W and 13.123L, Stewart Computational Chemistry, Colorado Springs, CO, USA, http://openmopac.net/, 2013.

[40] A. Pedretti, L. Villa, G. Vistoli, Journal of Computer-Aided Molecular Design 18 (2004) 167-173.

[41] G.A. Zhurko, D.A. Zhurko, Chemcraft (version 1.7, build 375, 2013), http://www.chemcraftprog.com.

[42] R Dennington, T. Keith, J. Millam, GaussView, Version 5.09, Semichem Inc., Shawnee Mission KS, 2013.

[43] A.V. Marenich, C.J. Cramer, D.G. Truhlar, Journal of Physical Chemistry B 113 (2009) 6378-6396.

[44] S.W.I. Siu, K. Pluhackova, R.A. Bockmann. Journal of Chemical Theory and Computation 8 (2012) 1459−1470.

[45] C.H. Bennett, Journal of Computational Physics 22 (1976) 245-268.

[46] C.L. Yaws (Ed.) Thermophysical Properties of Chemicals and Hydrocarbons Norwich, William Andrew Inc., New York, 2008.

[47] . D. van der Spoel, P. J. van Maaren, Journal of Chemical Theory and Computation 2 (2006) 1−11.

[48] P.M. Allen, D.J. Tildesley, Computer Simulations of Liquids, Clarendon, Oxford, U.K., 1987.

[49] B. Hess, H. Bekker, H.J.C. Berendsen, J.G.E.M. Fraaije, Journal of Computational Chemistry 18 (1997) 1463−1472.

[50] S. Pronk, S. Pall, R. Schulz, et al., Bioinformatics 29 (2013) 845-854.

[51] D. Honnery, D. Nguyen, J. Soria, Fuel 105 (2013) 247–257.

[52] A.W. Adamson, A.P. Gast, Physical Chemistry of Surfaces, 6th ed., Wiley, New York, 1997.

[53] T.K. Xia, U. Landman, Journal of Chemical Physics 101 (1994) 2498-2507.

[54] K. Nozaki, R. Saihara, K. Ishikawa, T. Yamamoto, Japanese Journal of Applied Physics 46 (2007) 761-769.

[55] R. Tuckermann, S. Bauerecker, B. Neidhart, Analytical and Bioanalytical Chemistry 372 (2002) 122-127.

[56] J. Frenkel, Zeitschrift für Physik 26 (1924) 117-138.